Eur. Phys. J. A **28**, 129–138 (2006)
DOI 10.1140/epja/i2005-10281-1

THE EUROPEAN PHYSICAL JOURNAL A

High-precision masses of $^{29-33}$Mg and the N = 20 shell "closure"

D. Lunney[a], G. Audi, C. Gaulard, M. de Saint Simon, C. Thibault, and N. Vieira

Centre de Spectrométrie Nucléaire et de Spectrométrie de Masse (CSNSM), IN2P3/CNRS-Université Paris Sud, Bâtiment 108, F-91405 Orsay, France

Received: 8 October 2005 / Revised: 19 February 2006 /
Published online: 19 June 2006 –
Communicated by J. Äystö

Abstract. High-precision mass measurements have been performed on the exotic magnesium isotopes $^{29-33}$Mg using the MISTRAL radiofrequency spectrometer, especially suited for very short-lived nuclides. This method, combined with the powerful tool of resonant laser ionization at ISOLDE, has provided a significant reduction of uncertainty for the masses of the most exotic Mg isotopes: a relative error of 7×10^{-7} was achieved for the weakly produced ^{33}Mg that has a half-life of only 90 ms. Moreover, the mass of ^{33}Mg is found to change by over 250 keV. Verifying and minimizing binding energy uncertainties in this region of the nuclear chart is important for understanding the lack of binding energy that is normally associated with magic numbers.

PACS. 21.10.Dr Binding energies and masses – 27.30.+t $20 \leq A \leq 38$ – 29.30.Aj Charged-particle spectrometers: electric and magnetic

1 Introduction

Shell structure is a pillar on which much of our knowledge and understanding of the nucleus rests. For some time now there has been evidence that this pillar is being eroded as the nuclear configuration tends towards the extreme in isospin. This is, of course, an allusion to the infamous "island of inversion," discovered from an anomaly in the binding energies of exotic Na isotopes with $N = 19$–21 [1, 2]. Binding energy that should normally be gained by the $N = 20$ shell closure is, in fact, unavailable. Further investigation of binding energies far from stability have shown that the $N = 8$ [3,4] and the $N = 28$ [5] shell closures also succumb. However, having disappeared, the shell closure may appear elsewhere for different elements —an apparent magic number *migration*. Such is the case for $N = 14$ [6], $N = 16$ [3,7], $Z = 16$ ($N = 30$) [8], as well as $N = 32$ [9–12] around $Z = 23$. Another magic appearance, claimed from γ-spectroscopy at $Z = 28$, $N = 40$ [13], is particularly interesting since there is no corroborating evidence from binding energy data (see [14]).

The island of inversion itself has since been the subject of intense experimental and theoretical scrutiny. A concise, historical review of the numerous expeditions devoted to its exploration is given in [15][1]. The inversion in question is the ordering of so-called "intruder" configurations: two-particle–two-hole ($2p$-$2h$) excitations formed by promoting a pair of *sd*-shell neutrons across the $N = 20$ shell gap into the normally-empty fp shell. Caurier *et al.* [18] give a detailed explanation of this phenomenon in which the intruders become the lowest in binding energy, mainly due to proton-neutron interactions. The intruders are also strongly deformed, resulting in a particularly interesting example of shape coexistence. Recent theoretical works have tackled the $N = 20$ shell from the perspective of a strongly attractive component of the spin-isospin part of the effective nucleon-nucleon interaction [19–22], as well as a mean-field model with separable monopole interaction [23] and Gogny-force mean field [24]. Promising efforts include important pairing correlations, either within the mean-field (HFB+QRPA) approach [25] or from Nuclear Field Theory [26] (in the case of $N = 8$).

Since the early work of Detraz *et al.* [27] and GuillemaudMueller *et al.* [28], β-spectroscopy studies of ^{33}Mg have followed at ISOLDE [29] and MSU [30]. The new tool of neutron knockout [31] gives detailed information concerning initial- and final-state wave functions. New results from inelastic scattering [32,6] have also become available in the meantime (see [33] for a summary of direct reactions performed in the $N = 20$ region). Precision measurements of the quadrupole moments of $^{26-31}$Na

[a] e-mail: lunney@csnsm.in2p3.fr

[1] Note that a reference was overlooked in that work (as in many papers) to an analysis based on binding energy differences by Heyde and Wood [16] who argued for shape coexistence in this region, a conclusion reached independently by the more often-cited shell model calculations of Warburton, Becker and Brown [17].

(at ISOLDE) by Keim *et al.* [34], using a β-NMR, optical pumping technique provide an important complementary perspective. The same technique has been used very recently to measure the magnetic moment of ^{31}Mg and unambiguously determine its spin [35], thus including it on the island of inversion.

A fine example of another complementary technique can be found in the suite of papers by Pritychenko *et al.*, [36–40] who performed γ-spectroscopy at MSU via Coulomb excitation. These studies have not only mapped the shore of the island of inversion, corroborating the one indicated by binding energies, but also furnished detailed nuclear structure information, especially concerning deformation. Coulomb excitation has also been performed on ^{30,32}Mg at GANIL [41] and on ^{34}Mg at RIKEN, where the energy of a 2^+ level [42] and the associated $B(E2)$ value indicate an even larger deformation than for ^{32}Mg [43]. Particularly interesting is the recent result on ^{30}Mg from REX-ISOLDE (advocating "safe" Coulomb excitation) [44] reporting a $B(E2)$ value compatible with the MSU result [36] yet significantly different than that of GANIL [41]. In the meantime, new 2^+ energies and $B(E2)$ measurements by Church *et al.* from MSU [45] are in accord with previous results for ^{32,34}Mg and confirm their presence on the island.

Also, the method of β-delayed γ spectroscopy was used by Tripanthi *et al.* [46] on ^{29}Na, "... defining the edge of the island of inversion for $Z = 11$." The $Z = 10$ "boundary" has also been patrolled using heavy-ion elastic scattering of ^{28}Ne by Iwasake *et al.* [47] and by γ spectroscopy of $^{25-29}$Ne from fragmentation by Belleguic *et al.* [48].

These new probes indeed shed more light on the behavior of shell closure strength even if the data are somewhat lacking in precision. It is therefore interesting to return to the original probe of the binding energy and make more precise measurements in order to put tighter constraints on the burgeoning theoretical approaches needed to interpret the data.

Mass measurements play an underpinning role in the determination of shell effects. It is often said that the atomic mass, through the binding energy $B(N, Z)$, embodies the net result of all interactions at work in the atom. This includes, of course, shell structure which is plainly visible when inspecting a graph of the two-neutron separation energy, defined by

$$S_{2n}(N, Z) = B(N, Z) - B(N - 2, Z) \qquad (1)$$

versus the number of neutrons, N for elements near the valley of stability. (The one-neutron separation energy $S_n(N, Z) = B(N, Z) - B(N - 1, Z)$ can also be used but the pairing effect must be avoided —see below.)

For a given Z, the general tendency for S_{2n} is to fall steadily as N increases. At the magic numbers (N_0) there is a sudden drop, corresponding to a loss in energy necessary to remove neutrons after a closed shell, before the more gradual fall resumes. The situation is well illustrated in fig. 1, where we show the variation with neutron number of S_{2n} for the light elements up to $Z \sim 50$. The magic number $N_0 = 50$ is quite evident. At $N_0 = 28$ we see

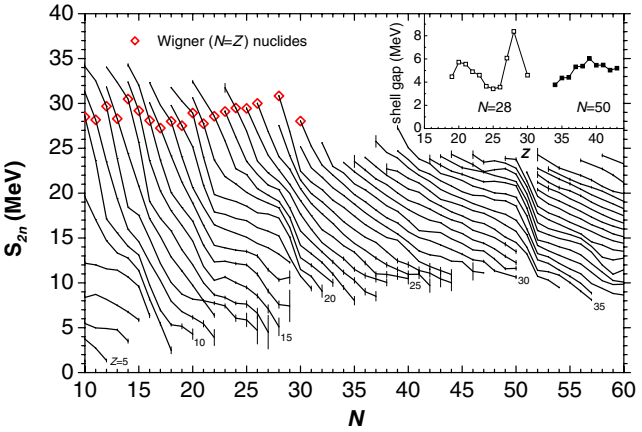

Fig. 1. Two-neutron separation energy S_{2n} for elements up to $Z \sim 50$, as a function of neutron number N. Data are taken from [74]. Inset: the shell gap Δ_{2n} for $N = 28$ and 50 as a function of Z.

a similar manifestation, though less pronounced than the $N_0 = 50$ case. At $N_0 = 20$, however, the situation is far from obvious. This is partly due to another embodiment of nuclear structure in the binding energy for $N = Z$ nuclides (marked by a diamond in fig. 1), the so-called Wigner effect where the same type of kink that manifests a shell closure can be seen. For $N = Z = 20$, the Wigner effect coincides with the $N = 20$ shell closure but for lighter elements, trends are difficult to discern. Note that, since S_{2n} is a derivative of the mass surface, two discontinuities will result from a change due to nuclear structure: one where the phenomenon occurs and another two neutrons later (by definition). For $Z = 15$–20, the corresponding second kink is visible at $N = 22$ however it is only for $Z = 15, 16$ that the shell closure kink itself at $N_0 = 20$ is perceivable and for lower Z, it seems to have melted away. Whence, the discovery of the famous island [1].

To quantify the strength of these magic numbers and the extent to which they are weakened[2] far from stability, we can examine the shell gap, a derivative of the neutron-separation energy surface, defined two ways:

$$\Delta_{2n}(N, Z) = S_{2n}(N, Z) - S_{2n}(N + 2, Z), \qquad (2)$$

$$\Delta_n(N, Z) = S_n(N, Z) - S_n(N + 1, Z). \qquad (3)$$

These two quantities can be used to examine different components of binding energy associated with closed shells *i.e.*, the $2p$-$2h$ energy for Δ_{2n} and $1p$-$1h$ energy for Δ_n.

A graph of $\Delta_{2n}(N, Z)$ is shown in the inset of fig. 1 for the magic numbers 28 and 50. The most prominent feature is the sharp peak at $N = Z = 28$, an impressive manifestation of the above-mentioned Wigner effect. Unfortunately, there is not enough experimental data to examine the Wigner effect for the $N = 50$ case, for which a mean shell gap of about 4–5 MeV is visible. The $N = 28$ shell gap decreases between the values $Z = 20$ and 28 but still remains relatively high (around 4 MeV) with a local maximum for the semi-magic case of $Z = 20$, a phenomenon

[2] The term "quenched" is often used in the literature.

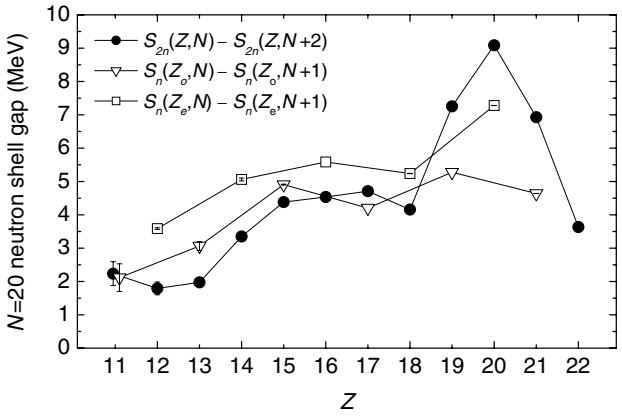

Fig. 2. Neutron shell gap defined by Δ_n and Δ_{2n} for $N = 20$, as a function of proton number Z.

referred to as "mutually-enhanced magicity" (see [49–51] for discussion).

The shell gap of interest here, $N = 20$, is plotted in fig. 2 as a function of Z both for $\Delta_{2n}(N, Z)$ and $\Delta_n(N, Z)$. Note that due to the large effect of pairing, two curves are plotted for $\Delta_n(N, Z)$: one for even Z and the other for odd Z. The feature of fig. 2 of particular relevance for this paper is the decline of the $N = 20$ shell gap approaching the dripline (*i.e.*, with decreasing Z), practically to extinction. $\Delta_n(N, Z)$ is important in this context, since it should indicate the neutron $1p$–$1h$ excitation energy for this closed shell since pairing amongst the p and h orbitals can be quite different. (By comparison, $\Delta_{2n}(N, Z)$ cancels the pairing energy amongst the $2p$ neutron pair and the $2h$ neutron pair.) If we examine these two quantities for $Z = 12$, we see that the shell gap is diminished in both cases.

Mass measurements first brought the phenomenon of shell weakening into the arena for study and naturally, continue to provide insight into questions on nuclear structure. Mass spectrometry, like the above-mentioned experimental techniques, has also enjoyed a renaissance (see *e.g.*, [51,52]). The MISTRAL[3] experiment has enabled us to return to the origin of this interesting physics problem by examining, with unprecedented accuracy, the neutron separation energies of some of the exotic nuclides on and around the island of inversion. In this paper we discuss mass measurements made by MISTRAL of the isotopes $^{29-33}$Mg at the ISOLDE radioactive beam facility [53], made possible by use of the ISOLDE laser ion source [54, 55]. The results are compared to previous (less accurate) measurements and discussed in light of the situation at $N = 20$.

2 Description of the MISTRAL spectrometer

As the MISTRAL spectrometer has been described elsewhere [15,56–62] only a brief explanation is given here.

[3] Mass measurements at ISOLDE using a Transmission and Radiofrequency spectrometer on-Line.

The mass is determined via the cyclotron frequency f_c of an ion of charge q and mass m, in a homogeneous magnetic field B:

$$f_c = \frac{q\,B}{2\pi\,m}\,. \tag{4}$$

The layout of MISTRAL is shown in fig. 3. The ion beam follows a two-turn helicoidal trajectory (fig. 3, central inset) to a secondary electron multiplier for counting. In order to obtain the high resolution needed for a precision mass measurement, a modulation of the longitudinal ion kinetic energy is effected by applying a time-varying (radiofrequency) voltage after one and three half-turns inside the magnetic field (fig. 3, right inset). The ions thus make one cyclotron orbit between the two modulations. The ions are maximally transmitted through the 0.4 mm exit slit when the net effect of the two modulations is zero. This happens when the radiofrequency voltage is an integer-plus-one-half multiple of the cyclotron frequency:

$$f_{RF} = \left(n + \frac{1}{2}\right)\, f_c. \tag{5}$$

The ion signal recorded over a wide frequency scan will exhibit transmission peaks that are evenly spaced at the cyclotron frequency (fig. 3, left inset). The resolving power $R = m/\Delta m$, will depend on the harmonic number n, the exit slit half-width w, and the modulation amplitude, D_m of the trajectory diameter [61]:

$$R = 2\pi n \frac{D_m}{w}\,. \tag{6}$$

The value of n is typically a few thousand and w is $\pm$ 0.2 mm. Depending on the ion velocity and modulator frequency response, D_m can vary between 3 and 6 mm. D_m is then proportional to the product of the modulation efficiency and the applied voltage. (See [57] for more detailed discussion.)

Figure 3 (left inset) shows a recorded transmission signal of the 60 keV ISOLDE ^{24}Mg beam over two successive harmonic values. As the RF power is increased, the voltage on the modulator increases (as the square root) and the conditions for transmission become more and more restrained, to the point where the wings of the transmitted ion signal can be completely suppressed. This happens when the modulation amplitude exceeds the width of the "phase definition slit," located between the entrance and exit slits, to eliminate modulated ion trajectories with large radial excursions. By closing the phase definition slit, it is possible to extend the zero-background zone which can be important in cases where isobaric contamination is present (as it was in the case of a previous measurement of ^{32}Mg [57,58]). Note however that this comes at a reduction of signal intensity: to have about half the area between harmonics background free requires paying about 60% in transmission and a factor of ten must be sacrificed to achieve a background-free zone of over 80%. The effect of the phase-defining slit is illustrated in fig. 3 (left inset). With the slit open (upper curve) the resolving power is 20000. By narrowing the slit (lower curve), a resolving

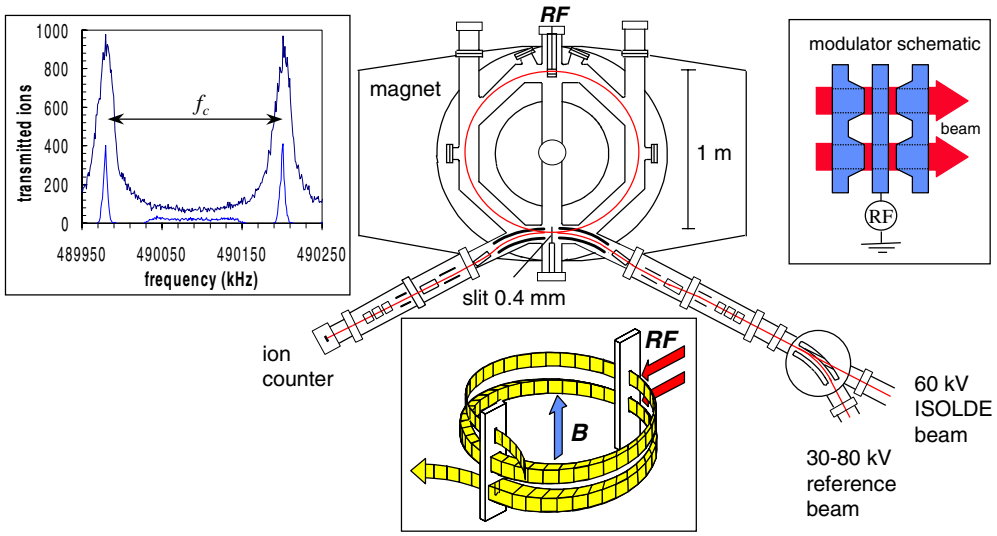

Fig. 3. Layout of the MISTRAL spectrometer (overhead view). The ion beams (coming from the right) are injected either from the ISOLDE beamline (at 60 keV) or from a reference ion source (variable energy). The central inset shows an isometric view of the trajectory envelope with the 0.4 mm injection slit followed by the first modulator after one-half turn, an opening to accommodate the modulated-ion trajectories after one-turn, the second modulator after three-half turns, and the exit slit. The right inset schematically illustrates the modulator electrode structure. The left inset shows the recorded signal of transmitted ^{24}Mg 60 keV ISOLDE ions as a function of modulation frequency for two RF power settings. The higher curve shows a resolving power of 20000 while the one with half the signal amplitude illustrates a resolving power of over 70000.

power of about 70000 is achieved together with a suppression of the peak tails and background. A resolving power up to 10^5 can be achieved this way if required. The resulting peak shape is approximately triangular [61,62].

The transmission of the spectrometer (through the four 0.4 mm × 5 mm slits that precisely define the nominal trajectory) is about 0.5% using the surface ionization reference source but can be lower than 0.01% using ISOLDE ion sources. In cases where higher resolving power is necessary (*e.g.*, isobaric contamination), the cost in transmission can be a further order of magnitude.

MISTRAL relies on a comparative measurement of a (generally stable) reference nuclide of well-known mass. The unknown mass m_x is transmitted through the spectrometer alternately with a reference mass m_r —without changing the magnetic field. Comparing masses in this way requires changing the transport energy of the reference beam, and with it, the voltages of all electrostatic elements in the spectrometer, according to the relation

$$m_r V_r = m_x V_x \,. \tag{7}$$

These comparisons are done in rapid succession (seconds) in order to eliminate error contributions due to the long-term drift of the magnetic field.

3 Production of the exotic Mg nuclides

Exotic nuclides are produced at the ISOLDE facility by nuclear reactions induced by an incident pulse of 1.0 or 1.4 GeV protons. These pulses, containing up to 3×10^{13} protons, are positioned within a timing structure called the PS supercycle, usually containing 12 pulses, spaced every 1.2 seconds. On average, about half of these pulses are sent to ISOLDE.

Once created, radioactive atoms diffuse into a chamber where they are ionized. Three possibilities exist depending on the chemical nature of the element in question: surface ionization, plasma-discharge, or resonant laser ionization. The target-ion source unit is operated on a high-voltage platform so that once ionized, the exotic nuclides are accelerated (normally to 60 keV) and mass separated. A general description of the ISOL technique is given in [53] and [51].

The data presented in this paper were recorded in September 2001 using the ISOLDE uranium carbide target combined with a resonant ionization laser ion source (RILIS) which delivers singly ionized, radioactive beams of exceptional chemical purity [54,55]. Some isobaric contamination from Na was present since it is surface ionized but the production cross-sections favor Mg by about a factor of 50 and the short Na half-lives suppress those yields by almost another order a magnitude. By blocking the laser beam, we performed a check measurement on ^{26}Na.

In a previous experiment [57,58], we used the plasma ion source in an attempt to measure the masses of several chemical species. Unfortunately, the isobaric contamination brought by the unselective plasma was overwhelming. In many cases, identification was even impossible due to the many possibilities of molecular sidebands as well as charge state. As a result, the resolving power of the spectrometer had to be increased to the point where a significant transmission loss made the measurements very difficult.

The derived production yield for ^{32}Mg was about 80000 per pulse with full proton intensity which corre-

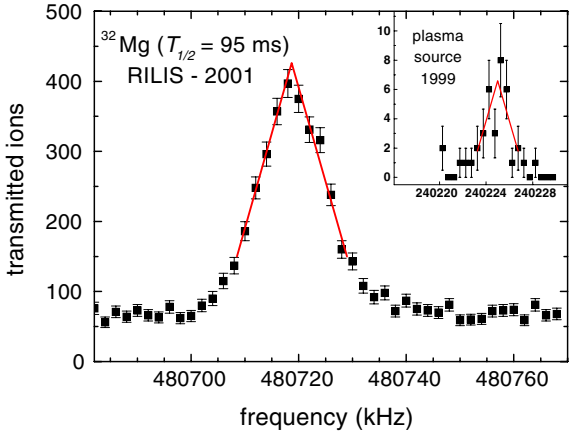

Fig. 4. Reconstructed peaks for ^{32}Mg using the laser ion source (RILIS) and (inset) using the plasma ion source [57,58]. These measurements are sums of series of (random) frequency steps with each step recorded after the impact of a proton pulse on the ISOLDE target. The mass resolving power for the RILIS case is about 30000 whereas 68000 was used for the plasma source due to presence of isobaric contamination (note the zero background as well). The statistics (in the maximum channel) correspond to 50 proton pulses (8 ^{32}Mg ions per pulse) for RILIS and 20 pulses (0.4 per pulse) for the plasma.

sponds to a normalized yield of 17000 ions/μC. A comparison of recorded mass peaks for ^{32}Mg using the plasmas and laser ion sources, is shown in fig. 4. The plasma peak (inset) was obtained by accumulating 20 pulses per frequency channel, corresponding to 0.4 detected ^{32}Mg ions/pulse at maximum peak amplitude. The RILIS peak, containing 400 counts at the maximum, was accumulated from 50 pulses, corresponding to 8 detected ^{32}Mg ions/pulse at maximum amplitude. This twenty-fold increase is due to several factors. First, the beam purity provided by RILIS allowed us to relax the resolving power, resulting in a gain of about four or five in transmission. (Note that while the plasma peak is less statistically abundant, its FWHM is half that of the laser peak and has zero background.) Assuming similar target performance (although considerable variation is possible), the RILIS performance would conceivably account for another factor of four-to-five improvement. The transmission of the laser-ionized ISOLDE beam through the spectrometer (without radiofrequency) was about three times better than the plasma-ionized beam, presumably due to a better ion source emittance. The remaining improvement may well be from a higher ionization efficiency of RILIS compared to plasma for Mg (see [55]). A higher modulation frequency was also used in this experiment, to achieve higher resolving power.

4 Results

The accumulated frequency spectra were analysed using a triangular fit [61] that includes beam intensity fluctuations and short-term magnetic drifts (the long-range drifts are corrected by frequent recording of reference mass spectra, as discussed above). The accuracy will depend on the resolving power, the statistics, the fluctuations and a systematic error component (discussed in detail in [63]).

4.1 Calibration

In our Na paper [15], we showed how the differences of our measurements relative to those of the atomic mass evaluation [64] revealed a dependency on the difference between the MISTRAL reference mass m_r and the ISOLDE unknown mass m_x, presumably due to imperfect superposition of the slightly differing trajectories in the magnetic field, known to have residual gradients [56]. The same systematic variation appeared in the present measurements. Several well-known masses were measured repeatedly throughout the experiment to determine the calibration. The calibration procedure has been the source of intense study both on- and off-line and as such, is the subject of an independent publication [63]. The new calibration law, developed in [63], takes the form

$$\Delta_x^{correct} = \Delta_x^{meas} - 2a(V_x - V_r)/(V_x + V_r) - b\,. \qquad (8)$$

The constant term b is added to correct for the offset which is observed between ISOLDE and MISTRAL beams of like mass.

In this experiment, a and b were determined by periodically measuring the precisely known masses ^{24,25,26,28}Mg as well as ^{23}Na with respect to the $A = 28$ reference beam of the singly ionized molecule ^{14}N^{14}N, throughout the run. The following values were obtained: $a = -445(20) \times 10^{-7}$ and $b = 1.2(2.8) \times 10^{-7}$. The details of the data analysis for this experiment, as well as the application of the new calibration law to previously published data, are all discussed in [63].

4.2 Mass values

The mass values are given in table 1, including all errors. The statistical and instrumental errors were relatively constant at about 4×10^{-7} while the calibration error added another 1–3 $\times 10^{-7}$ (see detailed analysis in [63]).

The calibrant masses show excellent agreement with the 1995 "Atomic Mass Evaluation" (AME'95) [64] thereby confirming the validity of the method and calibration law. The relative precision for these masses is between 2 and 5 $\times 10^{-7}$ while for the measured masses it falls between 3 and 7 $\times 10^{-7}$.

4.3 Evaluation

A significant improvement in the mass values has been achieved, especially far from stability where almost an order of magnitude is reached.

For the AME'95 [64], five different experimental results existed with which the mass of ^{29}Mg could be derived: 1) the β-decay to ^{29}Al [65]; 2) the ^{26}Mg(^{11}B, ^{8}B)^{29}Mg reaction [66]; 3) the ^{26}Mg(^{18}O, ^{15}O)^{29}Mg reaction [67]; 4) the ^{18}O(^{13}C, $2p$)^{29}Mg reaction [68]; 5) the

Table 1. MISTRAL results with the RILIS source. The first column corresponds to the nuclidic name. Column 2 gives the absolute deviations from the AME'95 mass table [64], and column 3, the new MISTRAL mass excess. Note that these values supersede those listed in the recent AME'03 mass table [74] which were based on a preliminary analysis using the old calibration law.

Nuclide	δm_x (keV)	Mass excess (keV)
Calibrant masses		
^{23}Na	2.6(5.2)	
^{24}Mg	−4.0(5.4)	
^{25}Mg	−3.9(6.7)	
^{26}Mg	5.7(5.8)	
^{28}Mg	−5.0(11.2)	
Measured masses		
^{29}Mg	53	−10608(15)
^{30}Mg	−10	−8892(13)
^{31}Mg	26	−3190(16)
^{32}Mg	−120	−915(20)
^{33}Mg	−257	4947(22)

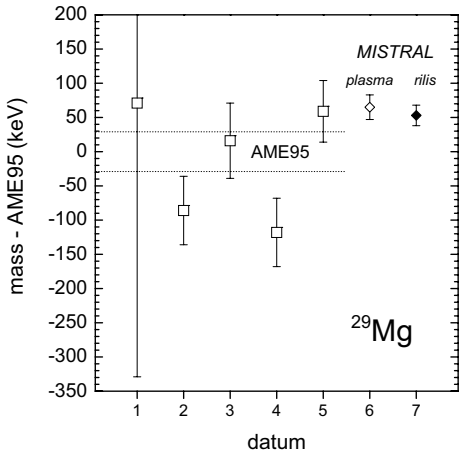

Fig. 5. Difference of the 1995-evaluated ^{29}Mg mass and that measured by different experiments: 1) from β-decay to ^{29}Al [65]; 2) the ^{26}Mg(^{11}B, ^{8}B)^{29}Mg reaction [66]; 3) the ^{26}Mg(^{18}O, ^{15}O)^{29}Mg reaction [67]; 4) the ^{18}O(^{13}C, $2p$)^{29}Mg reaction [68]; 5) the ^{26}Mg(^{18}O, ^{15}O)^{29}Mg reaction [69]; 6) MISTRAL result from [57,58], reanalyzed in [63]; 7) result from this work (and [63]). The AME'95 [64] error band, derived from data 2), 3) and 5) is also shown.

^{26}Mg(^{18}O, ^{15}O)^{29}Mg reaction [69]. These results are illustrated in fig. 5 with respect to the AME'95 [64] ^{29}Mg mass, determined from data 2), 3) and 5). Also shown is 6) the MISTRAL result from [58,57], reanalyzed in [63] and 7) the result from this work (and [63]). The decay result is no longer used due to its large error and the reaction results roughly agree. It is interesting that 4) had not been used in AME'95. The recommended mass value in [64] has moved by about 60 keV and is now a factor a two more precise.

Table 1 shows that the mass of ^{32}Mg is about 120 keV more bound, and that of ^{33}Mg is 257 keV more bound than the AME'95 values. To probe the reasons for this we examine in fig. 6 the results of all experiments in which the masses of $^{30-33}$Mg were determined by direct techniques as well as the (overall) recommended mass values from the AME'95 [64], obtained from time-of-flight measurements at two installations: LAMPF [70,71] and GANIL [72,73].

Also compared in fig. 6 is the 1999 MISTRAL measurement for ^{32}Mg using the plasma ion source [57,58]. Following that experiment, a discharge was discovered on the electrostatic injection septum and it is reasonable to assume that maintaining a congruence between the two trajectories would be impossible. Despite this problem, the 1999 results are in agreement with the new results, performed under quite different (and better) conditions. Moreover, the reanalysis of those results [63] (marked by an asterisk) shows an even better agreement.

Overall, the new MISTRAL measurements are quite compatible, not only with the previous individual measurements but also the recommended values from the 1995 evaluation (the slight deviation for the exotic ^{33}Mg is less than 2σ). However, the uncertainty of the MISTRAL masses is five to seven times better than in the AME'95. As such, in the new AME'03 evaluation [74], the MISTRAL masses now account for 100% of the weight of the recommended values due to their superior precision. (Note that the values reported here supersede those listed in AME'03 [74] which were based on a preliminary analysis using a different calibration law.) In addition to the TOFI and SPEG values, some older reaction Q values (using ^{18}O and ^{11}B projectiles on ^{26}Mg targets) and Q_β values from exotic Na nuclides, no longer contribute due to their large uncertainties [74].

Any mass measurement has need of a calibration. In many cases, exotic masses are derived using extrapolations from nuclides closer to stability. Recent measurements of neutron-rich Mg isotopes (among others) at GANIL were reported in [5]. In that work, the (AME'95) mass of ^{33}Mg was used as a *calibrant* for the measured masses of $^{34-36}$Mg. If the calibration is off by 250 keV, this could have considerable impact on the mass values further from stability. In fact, the evaluators of the AME'03, considered that the masses of $^{34-36}$Mg deviated too much from smooth trends and consequently replaced them by systematic values.

5 Discussion

5.1 Comparison to mass models

Mass models can cover a wide spectrum, in terms of applicability as well as in terms of physics input. They can broadly be described as being either local in character, typically containing many parameters (adjusted to experimental masses) and predicting unknown masses with relatively good accuracy very close to the region where the ajustment was made. Global models tend to have fewer ajustable parameters and more physics. While this can make the predictions somewhat worse, the extrapolation to further unknown regions tends to be more reliable.

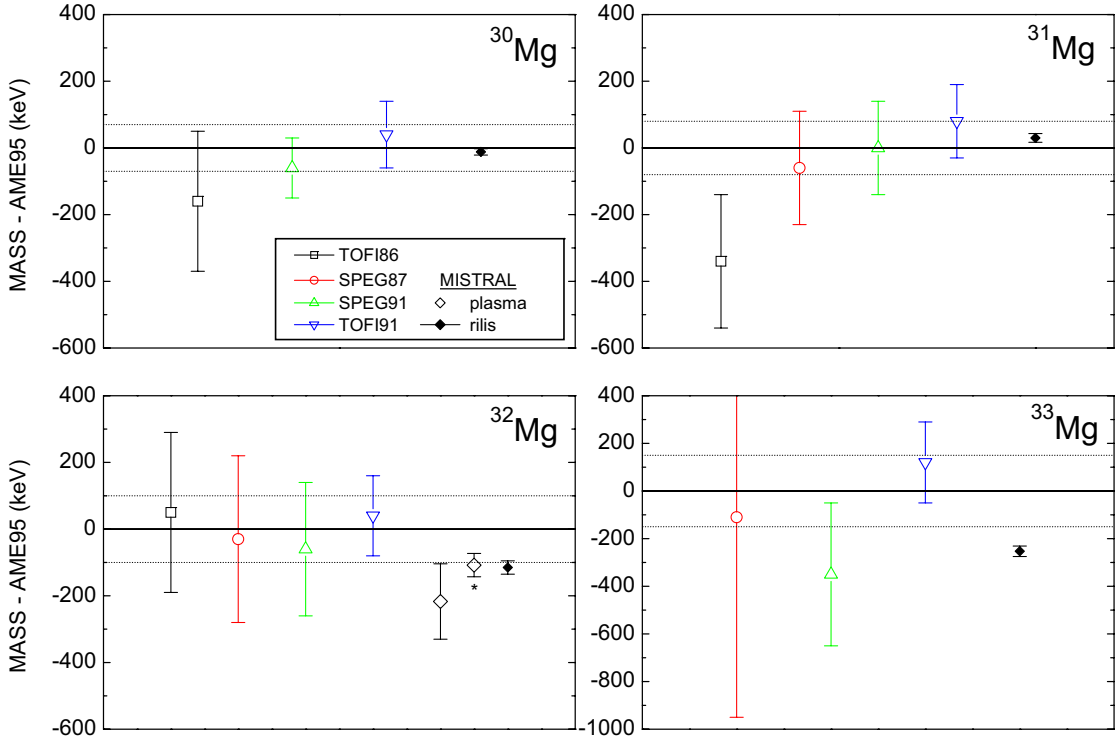

Fig. 6. Comparison of the results of mass spectrometry experiments in which the masses of $^{30-33}$Mg have been determined: time-of-flight measurements (TOFI) at LAMPF [70,71] and GANIL [72,73] and RF mass spectrometry ([57,58,63] and this work).

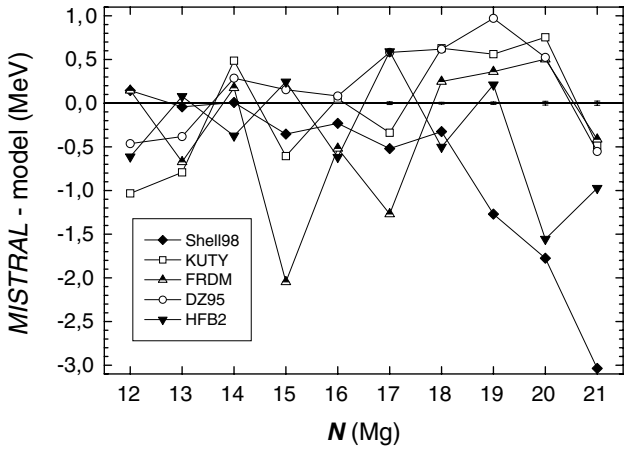

Fig. 7. Comparison of the newly measured Mg masses compared to predictions of several mass models (Shell98 [18], KUTY [77], FRDM [75], DZ95 [76], HFB-2 [78]).

See [51] for a general classification, explanation and comparison of the various types of models.

Predictions for Mg masses from the macroscopic-microscopic Finite Range Droplet Model (FRDM) of Moeller *et al.* [75], microscopic shell model calculations of Caurier *et al.* [18], as well as the microscopic mass formula of Duflo and Zuker (DZ95) [76], Koura *et al.* (KUTY) [77], and HFB-2 [78] are shown in fig. 7, compared to the experimental values determined in this work. Perhaps the most striking feature of fig. 7 is the odd-even staggering compared with experiment indicating a major problem in how the pairing force is handled by mass formulas in general (see discussion in [51]). The shell model calculations seem not to be affected by this, however after $N = 18$ they veer off towards the underbound. This is very illustrative of restricted mathematical basis and coupling with continuum, two major problems besetting the shell model. The pairing problem seems quite pronounced for the FRDM and KUTY formulas while it is much less acute for DZ. Interestingly, the KUTY, FRDM and DZ formulas all show the same behavior crossing the $N = 20$ shell. Whether this shell is closed or not, the microscopic HFB-2 formula shows a strong underbinding. But on the whole, its 705 keV rms deviation for the Mg isotopes is comparable to that of KUTY (627 keV) and even better than FRDM (848 keV)[4]. At 521 keV, the DZ formula does the best job in this region —as it does for the entire mass table (see [51]). The rms error for the shell model calculations is 1.2 MeV.

5.2 General discussion

The impact of precision mass measurements on the question of shell opening is not particularly clear-cut. Like many results, they bring pieces of a large puzzle and in other cases, masses provide overall constraints that need

[4] Note, however, that the parameters of HFB-2 were adjusted to a more extensive data set (see [51,79,78]).

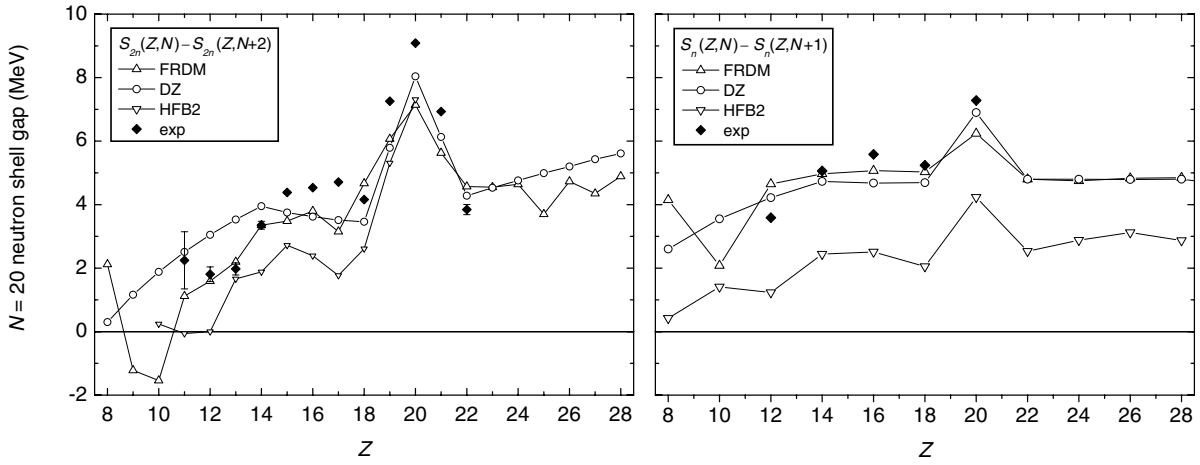

Fig. 8. Shell gap quantities Δ_{2n} (left) and Δ_n (right) calculated from the present experimental data plus those of [74] compared with nuclear models (FRDM [75], DZ95 [76], HFB-2 [78]).

to be satisfied by level assignments, half-life calculations, or model predictions.

The shell gap was discussed in the introduction and the mass surface discussed in this context. In the light region of $N = 20$, it is particularly difficult to disentangle the various structure effects from the mass surface since things change so quickly for small numbers of nucleons. In fig. 8 the $N = 20$ shell gap calculated using eqs. (2) (left) and (3) (right) are compared to predictions of some of the above models. This is an interesting exercise since the shell gap is calculated from mass *differences*. It might be possible for a model to follow the microscopic behavior fairly well despite having a large, but relatively constant difference.

Conspicuous in each panel of fig. 8 is the large shell gap for $N = Z = 20$, a Wigner nuclide which is also doubly magic. All three models underestimate this effect (by at least 1 MeV). Contrary to the absolute mass values, the FRDM seems to follow the shell gap (*i.e.*, mass difference) data relatively well. The shell weakening is very sudden below $Z = 11$, moreover becoming negative! DZ95, despite its success with heavier shell gaps, predict a more gradual erosion of the shell gap. The HFB-2 results show the shell weakening already at $N = 13$ and seem to be systematically lower than experiment.

The criterion for deciding whether a given nuclide is part of the island of inversion or not, is somewhat subjective. The older arguments derived from binding energies (*e.g.*, [17]) could be questioned on one hand, by more precise mass data that has since become available [15,74], and on the other hand by more recent shell model calculations [18] that indicate a departure from the "universal *sd* shell" already at $N = 19$ for Na (see discussion in [15] and more appropriately, in [22]). This conclusion is supported by the quadrupole moment measurements from β-NMR [34]. The very recent results using β-NMR at ISOLDE for the magnetic moment and unambiguous ground-state spin of ^{31}Mg, coupled with state-of-the-art shell model calculations, also indicate the invasion of the intruder orbits at $N = 19$ [35].

The shell model calculations that accompanied the β-spectroscopy of ^{33}Mg in [29] included only an approximation of the mixing between $0p$-$0h$ and $2p$-$2h$ configurations. This apparently leads to an excited state of different instrinsic stucture than that described by the complementary Coulomb excitation studies in [39], namely that the excited state in question is rotational in nature, leading to different conclusions regarding the ground state spin and deformation. A more recent β-decay study of ^{33}Mg by [30] has also made different assumptions regarding the configuration of the ground state. Further discussion of these differing conclusions is beyond the scope of this paper. However, the importance of different, complementary experimental techniques is clear enough. Interestingly, Nummela *et al.* [29] report that the uncertainties related to building the level schemes for ^{33}Mg are dominated by the error on the ^{33}Na-^{33}Mg Q-value. In the same vein, Mantica *et al.* [10,11] remind us that the errors in half-life calculations are dominated by Q-value uncertainties.

The binding energy associated with shell effects is very small compared to, for example, the surface energy, but is decisive in the configuration of the last nucleons. Hence, the importance of precision mass measurements is not understated.

6 Conclusion

We have discussed the results for the masses of neutron-rich Mg isotopes using a new technology for mass measurements that is especially suitable for very short-lived species. The results represent the most accurate measurements to date for the short-lived nuclides $^{29-33}$Mg which lie in the so-called "island of inversion" around the $N = 20$ shell closure. We have examined this phenomenon in light of recent mass models, find that if evanescent shell stability is to be properly included for studying, for example, the astrophysical r process, then improvements will have to be made. This translates to a requirement for more mass data, of high precision, as far as possible from stability.

Efforts are currently underway to increase the sensitivity of the spectrometer. These improvements will allow MISTRAL to realize its full potential for accurate mass measurements of the shortest-lived nuclides at the drip line.

We would like to acknowledge the expert technical assistance of G. Conreur, M. Jacotin, J.-F. Képinski and G. Le Scornet from the CSNSM. We thank H. Doubre for his assistance during the experiment. We also express our sincere gratitude to V.N. Fedoseyev and D.V. Fedorov for the superbly reliable operation of the laser ion source, to T. Giles, U. Köster, H. Fynbo and L. Weissman for their symbiotic help in tuning the ISOLDE HRS separator, the ISOLDE technical group and the ISOLDE Collaboration. The MISTRAL program is supported by France's IN2P3 and by the EU research network NIPNET (contract number HPRI-CT-2001-50034). The work at ISOLDE was partially supported by the EU RTD program "Access to Research Infrastructures", under contract number HPRI-CT-1998-00018.

References

1. C. Thibault, R. Klapisch, C. Rigaud, A.M. Poskanzer, R. Prieels, L. Lessard, W. Reisdorf, Phys. Rev. C **12**, 644 (1975).
2. X. Campi, H. Flocard, A.K. Kerman, S. Koonin, Nucl. Phys. A **251**, 193 (1975).
3. A. Ozawa *et al.*, Phys. Rev. Lett. **84**, 5493 (2000).
4. S. Shimoura *et al.*, Phys. Lett. B **560**, 31 (2003).
5. F. Sarazin *et al.*, Phys. Rev. Lett. **84**, 5062 (2000).
6. E. Becheva *et al.*, Phys. Rev. Lett. **96**, 012501 (2006).
7. A. Obertelli *et al.*, Phys. Rev. C **71**, 024304 (2005).
8. R. Kanungo, I. Tanihata, A. Ozawa, Phys. Lett. B **528**, 58 (2002).
9. J.I. Prisciandoaro *et al.*, Phys. Lett. B **510**, 17 (2001).
10. P.F. Mantica *et al.*, Phys. Rev. C **67**, 014311 (2003).
11. P.F. Mantica *et al.*, Phys. Rev. C **68**, 014311 (2003).
12. D.E. Appelbe *et al.*, Phys. Rev. C **67**, 034309 (2003).
13. O. Sorlin *et al.*, Phys. Rev. Lett. **88**, 092501 (2002).
14. C. Guénaut *et al.*, Eur. Phys. J. A **25**, s01, 33 (2005).
15. D. Lunney, G. Audi, H. Doubre, S. Henry, C. Monsanglant, M. de Saint Simon, C. Thibault, C. Toader, C. Borcea, G. Bollen, the ISOLDE Collaboration, Phys. Rev. C **64**, 054311 (2001).
16. K. Heyde, J.L. Wood, J. Phys. G **17**, 135 (1991).
17. E.K. Warburton, J.A. Becker, B.A. Brown, Phys. Rev. C **41**, 1147 (1990).
18. E. Caurier, F. Nowacki, A. Poves, J. Retamosa, Phys. Rev. C **58**, 2033 (1998).
19. Y. Utsuno *et al.*, Phys. Rev. C **60**, 054315 (1999).
20. T. Otsuka *et al.*, Phys. Rev. Lett. **87**, 082502 (2001).
21. T. Suzuki, R. Fujimoto, T. Otsuka, Phys. Rev. C **67**, 044302 (2003).
22. Y. Utsuno *et al.*, Phys. Rev. C **70**, 044307 (2004).
23. P.D. Stephenson, J. Rikovska-Stone, M.R. Strayer, Phys. Lett. B **545**, 291 (2002).
24. S. Péru, M. Girod, J.F. Berger, Eur. Phys. J. A **9**, 35 (2000).
25. M. Yamagami, N. Van Giai, Phys. Rev. C **69**, 034301 (2004).
26. G. Gori *et al.*, Phys. Rev. C **69**, 041302(R) (2004).
27. C. Détraz, M. Langevin, M.C. Goffri-Kouassi, D. Guillemaud, M. Epherre, G. Audi, C. Thibault, F. Touchard, Nucl. Phys. A **394**, 378 (1983).
28. D. GuillemaudMueller, C. Détraz, M. Langevin, F. Naulin, M. de Saint Simon, C. Thibault, F. Touchard, M. Epherre, Nucl. Phys. A **426**, 37 (1984).
29. S. Nummela *et al.*, Phys. Rev. C **64**, 054313 (2001).
30. A.C. Morton, P.F. Mantica *et al.*, Phys. Lett. B **544**, 274 (2002).
31. J. Enders *et al.*, Phys. Rev. C **65**, 034318 (2002).
32. W. Mittig *et al.*, Eur. Phys. J. A **15**, 157 (2002).
33. T. Motobayashi, Eur. Phys. J. A **15**, 99 (2002).
34. M. Keim, in *Proceedings of the International Conference on Exotic Nuclei, Atomic Masses (ENAM98)*, edited by B.M. Sherrill, D.J. Morrissey, C.N. Davids, AIP Conf. Proc. **455** (AIP, New York, 1998) p. 50.
35. G. Neyens, M. Kowalska, D. Yordanov *et al.*, Phys. Rev. Lett. **94**, 022501 (2004).
36. B.V. Pritychenko *et al.*, Phys. Lett. B **461**, 322 (1999).
37. B.V. Pritychenko *et al.*, Phys. Rev. C **63**, 011305(R) (2000).
38. B.V. Pritychenko *et al.*, Phys. Rev. C **63**, 047308 (2001).
39. B.V. Pritychenko *et al.*, Phys. Rev. C **65**, 061304(R) (2002).
40. B.V. Pritychenko *et al.*, Phys. Rev. C **66**, 024325 (2002).
41. V. Chisté *et al.*, Phys. Lett. B **514**, 233 (2001).
42. K. Yoneda *et al.*, Phys. Lett. B **499**, 233 (2001).
43. H. Iwasaki *et al.*, Phys. Lett. B **522**, 227 (2001).
44. O. Niedermaier *et al.*, Phys. Rev. Lett. **94**, 172501 (2005).
45. J.A. Church *et al.*, Phys. Rev. C **72**, 054320 (2005).
46. V. Tripanthi *et al.*, Phys. Rev. Lett. **94**, 162501 (2005).
47. H. Iwasaki *et al.*, Phys. Lett. B **620**, 118 (2005).
48. M. Belleguic *et al.*, Phys. Rev. C **72**, 054316 (2005).
49. N. Zeldes, T.S. Dumistrescu, H.S. Köhler, Nucl. Phys. A **399**, 11 (1983).
50. M. Bender, G. Bertsch, P.-H. Heenen, Phys. Rev. Lett. **94**, 102503 (2005).
51. D. Lunney, J.M. Pearson, C. Thibault, Rev. Mod. Phys. **75**, 1021 (2003).
52. D. Lunney, G. Audi, H.-J. Kluge (Editors), *Proceedings of the 2nd Euroconference on Atomic Physics at Accelerators: Mass Spectrometry (APAC2000), Cargèse, France*, Hyperfine Interact. **132** (2001).
53. E. Kugler, Hyperfine Interact. **129**, 23 (2000).
54. V.I. Mishin *et al.*, Nucl. Instrum. Methods B **73**, 550 (1993).
55. U. Koester, Nucl. Phys. A **701**, 441 (2002).
56. A. Coc *et al.*, Nucl. Instrum. Methods A **305**, 143 (1991).
57. D. Lunney *et al.*, Hyperfine Interact. **132**, 299 (2001).
58. C. Monsanglant, Doctoral Thesis, Université Paris-Sud, Orsay (2000); `http://tel.ccsd.cnrs.fr/tel-00002383`.
59. M. de Saint Simon *et al.*, Phys. Scr. T **59**, 406 (1995).
60. M.D. Lunney *et al.*, Hyperfine Interact. **99**, 105 (1996).
61. A. Coc *et al.*, Nucl. Instrum. Methods A **271**, 512 (1988).
62. N. Vieira, Doctoral Thesis, Université Paris VI, Paris (2002); `http://tel.ccsd.cnrs.fr/tel-00002578`.
63. C. Gaulard, G. Audi, C. Bachelet, D. Lunney, M. de Saint Simon, C. Thibault, N. Vieira, Nucl. Phys. A **766**, 52 (2006).
64. G. Audi, A.H. Wapstra, Nucl. Phys. A **595**, 409 (1995).
65. D.R. Goosman, C.N. Davids, D.E. Alburger, Phys. Rev. C **8**, 1331 (1973).
66. D.K. Scott *et al.*, Phys. Rev. Lett. **33**, 1343 (1974).

67. I. Paschopoulos *et al.*, Phys. Rev. C **18**, 1277 (1978).
68. A.D. Panagiotou *et al.*, Z. Phys. A **302**, 117 (1981).
69. L.K. Fifield *et al.*, Nucl. Phys. A **437**, 141 (1985).
70. D.J. Vieira *et al.*, Phys. Rev. Lett. **57**, 3253 (1986).
71. X.G. Zhou *et al.*, Phys. Lett. B **260**, 285 (1991).
72. A. Gillibert *et al.*, Phys. Lett. B **192**, 39 (1987).
73. N.A. Orr *et al.*, Phys. Lett. B **258**, 29 (1991); **271**, 468 (1991)(E).
74. G. Audi, A.H. Waptstra, C. Thibault, Nucl. Phys. A **729**, 337 (2003); A.H. Waptstra, G. Audi, C. Thibault, Nucl. Phys. A **729**, 129 (2003).
75. P. Möller, J.R. Nix, W.D. Myers, W.J. Swiatecki, At. Data Nucl. Data Tables **59**, 185 (1995).
76. J. Duflo, A.P. Zuker, Phys. Rev. C **52**, R1 (1995).
77. H. Koura, M. Uno, T. Tachibana, M. Yamada, Nucl. Phys. A **674**, 47 (2000).
78. S. Goriely, M. Samyn, J.M. Pearson, P.-H. Heenen, F. Tondeur, Phys. Rev. C **66**, 024326 (2002).
79. G. Audi, A.H. Wapstra, private communication (2001).